Catal Lett (2008) 123:198–206
DOI 10.1007/s10562-008-9448-y

Titania-Supported Gold Catalysts: Comparison between the Photochemical Phenol Oxidation and Gaseous CO Oxidation Performances

M. A. Centeno · M. C. Hidalgo · M. I. Dominguez · J. A. Navío · J. A. Odriozola

Received: 23 January 2008 / Accepted: 13 February 2008 / Published online: 6 March 2008
© Springer Science+Business Media, LLC 2008

Abstract A series of Au/TiO_2 samples with gold loadings ranging from 0.11% to 1.26% have been prepared by deposition–precipitation, characterised by means of XRD, S_{BET}, XRF, TEM, XPS and DR UV–Vis techniques and tested in the gaseous CO oxidation and photocatalytic degradation of phenol in aqueous media. The catalytic performances of the solids on both reactions depend on the gold content. Besides this, the gold particle size plays a determinant role in the catalytic activity for the CO reaction, but apparently its influence on the photocatalytic activity appears to be negligible and only very small gold particles seem to participate on the photocatalytic process. On the other hand, the electronic properties of the solids, measured by its band gap energy, are a key factor in the photochemical activity but do not have a clear influence in the CO oxidation reaction.

Keywords Titania-supported-gold catalysts · CO oxidation · Photocatalysis · Phenol oxidation

1 Introduction

In the latest years the number of works focussed on gold-containing catalysts has increased exceptionally, due to their very high activity at low temperature in a large number of different catalytic reactions, in particular, oxidation ones [1, 2]. Most of the catalytic reactions reported are gaseous ones, for instance, hydrogenation of carbon oxides and hydrocarbons, NO reduction, hydrochlorination of ethylene, propene epoxidation, water–gas shift, CO oxidation and the oxidation of volatile organic compounds (VOCs) [1, 3–6]. In all these reactions, the catalytic activity and stability of gold catalysts have been described to depend on the nature of the support, the size and distribution of gold particles and the properties of the contact surface gold-support. Among the large number of gold catalysts tested, those using TiO_2 as support are majority [7–11]. The use of gold catalysts in catalytic liquid phase oxidations is more recent. It has been reported, for instance, the oxidation of polyols [12] and glycerol [13]. Additionally, as heterogeneous photocatalysts, gold supported on titania, has been subject of a recent interest [14–17]. TiO_2 photocatalysis is an attractive and very effective technique for the complete destruction of contaminants in both aqueous [18–20] and gaseous phase [21–22]. The improvement of the photocatalytic activity of TiO_2 continues to be one of the most important subject of research in the field of photocatalysis and the surface modification of titania with gold has been proven to be an efficient way to enhance its photocatalytic activity [14–16, 23, 24] by increasing the efficiency of charge separation and decreasing the charge carrier recombination speed, one of the negative attributes of titania as a photocatalyst. On the other hand, the photocatalytic activity of titania has been described to be strongly influenced by morphological and structural parameters, such as its crystal structure, surface area, particle size distribution, porosity, band gap, and surface hydroxyl group density [25, 26].

In this paper, we study the catalytic behaviour of a series of gold supported on TiO_2 P25 samples with gold loadings ranging from 0.11% to 1.26%, in the gaseous CO oxidation and in the photocatalytic degradation of phenol in aqueous

M. A. Centeno (✉) · M. C. Hidalgo · M. I. Dominguez · J. A. Navío · J. A. Odriozola
Instituto de Ciencia de Materiales de Sevilla, Centro Mixto CSIC-Universidad de Sevilla, Avda Americo Vespucio s/n, 41092 Sevilla, Spain
e-mail: centeno@icmse.csic.es

media, in order to investigate which are the characteristics of the gold deposited on the titania surface that control and influence both reactions. We have selected a commercial TiO_2 P25 solid as titania support, because the junction between its two constituent phases (anatase and rutile) already provides a very good path for electron–hole separation minimising the influence of this mechanism on the catalytic activity and allowing to discern the improve of the activity due to gold introduction.

2 Experimental

2.1 Catalysts

Gold catalysts were synthesised by deposition–precipitation. The adequate amount of $HAuCl_4 \cdot 3H_2O$ (Alfa, 99.99% pure) to obtained 0.1, 0.2, 0.25, 0.5, 1 and 2% w/w Au in the final catalysts was dissolved in 100 mL of deionised water and the pH of the solution adjusted to 7.0 by addition of NaOH 0.1 M. The solution was heated to 70 °C and then, the support (as received TiO_2 Degussa P25) was added and kept under continuous stirring for 1 h. The samples obtained were washed with distilled water several times (until disappearance of chloride and Na^+), and dried overnight at 100 °C in an oven.

2.2 Characterisation Techniques

X-ray diffraction (XRD) analysis was performed on a Siemens diffractometer D500. Diffraction patterns were recorded with Cu Kα radiation (40 mA, 40 kV) over a 2θ-range of 10° to 70° and a position-sensitive detector using a step size of 0.05° and a step time of 1 s.

The textural properties were studied by N_2 adsorption measurements at liquid nitrogen temperature. The experiments were carried out in Micromeritics ASAP 2010 equipment. Before analysis, the samples were degassed for 2 h at 150°C in vacuum.

Gold content of the samples was determined by X-ray fluorescence spectrometry (XRF) in a Siemens SRS 3000 sequential spectrophotometer with a rhodium tube as the source of radiation. XRF measurements were performed onto pressed pellets (sample included in 10 wt% of wax).

Transmission electron microscopy (TEM) observations were carried out in a Philips CM200 microscope operating at 200 kV. The samples were dispersed in ethanol by sonication and dropped on a copper grid coated with a carbon film.

Diffuse reflectance UV–Vis spectra of the solids diluted in $BaSO_4$ were recorded at room temperature on a Shimadzu UV-2101PC spectrometer equipped with an integrating sphere and using $BaSO_4$ as reference. They are presented normalised in Kubelka–Munk mode without any other transformation.

The X-ray photoelectron spectroscopy (XPS) analyses were obtained in an ultra high vacuum chamber (UHV) at a pressure around 10^{-9} Torr, to which an energy electron analyser (VG 100 AX) was fitted, using a Mg Ka X-ray source operating at 15 kV and 20 mA. Before analyses, the samples were degassed overnight (10^{-7} Torr). The binding energy was calculated with respect to the C–(C,H) component of the C_{1s} adventitious carbon fixed at 284.6 eV. The spectra were decomposed according to a commercial fitting program (VGX900) with a Gussian/Lorentzian ratio of 85/15 and after subtracting a Shirley-type nonlinear baseline. The atomic ratios were calculated from the relative intensity corrected by the Scotfield factor of each atom.

2.3 Catalytic Activity

The catalytic tests of CO oxidation were carried out in a conventional continuous flow U-shape glass reactor working at atmospheric pressure where 80 mg of sample is placed over glass wools. A thermocouple in contact with the sample assures the right measure of temperature. The reactor was surrounded by an electrical furnace equipped with a temperature programmer. The feed mixtures were prepared using mass flow controllers (Bronkhorst). The reaction was followed by mass spectrometry, using a Balzers Thermostar benchtop mass spectrometer controlled by the software Balzers Quadstar 422 with capabilities for quantitative analysis.

The light-off curves of CO oxidation (500 °C, 5 °C/min) were obtained with a mixture 3.4% CO and 21% O_2 balanced by He at a total flow rate of 42 mL/min. Empty reactor (without sample) shows no activity under such conditions.

Photocatalytic runs were performed in a Pyrex immersion well reactor with a reaction volume of 450 mL. UV illumination of the reaction solutions was provided by a medium pressure Hg lamp (400 W) supplied by Applied Photophysics. A photon flow of 2.6×10^{-7} Einstein L^{-1} s^{-1} was calculated by using the chemist actinometer Aberchrome 540 [27]. The photocatalytic activity of the samples (1 g/L) was tested for the reaction of photooxidation of phenol at natural water pH with an initial concentration of 50 ppm, using oxygen flow to produce homogeneous suspensions. Prior to illumination, the suspensions were stirred in the dark for 20 min for catalyst–substrate equilibration. Phenol degradation profiles as function of the illumination time (2 h) were followed by UV–Vis spectrometry through the evolution of phenol characteristic 270 nm band, using filtered aliquots periodically removed from the suspension (Millipore Millex25 0.45 mm membrane filter). The activity

of the different samples was estimated by using initial degradation rates as degradation profiles followed zero order kinetics during this stage. Blank experiments were performed without any catalyst as well as in absence of illumination without observable change in the initial concentration of phenol in both cases.

3 Results and Discussion

3.1 Characterisation

Table 1 shows the code, gold content and textural properties of the prepared solids. All solids maintain the initial specific surface area BET of the titania P25 support (50 m^2 g^{-1}) except the one with the highest gold content (1.26% Au) which presents a little decrease in this value (10%). However, the introduction of gold induces an appreciable increase in the average pore size and in the total pore volume of the samples. These effects have been yet reported on gold supported MCM-41 and MCM-48 zeolites [28] and on gold supported on alumina and ceria [29], and explained by the expansion of the mesoporous structure of the support because of the introduction of gold nanoparticles inside the structure.

The XRD patterns of the studied solids are present in Fig. 1. The relative proportion of phases of TiO_2 (20% rutile, 80% anatase) as well as the average size of the crystalline domains of the titania P25 support are maintained in the gold supported samples.

No reflections due to polycrystalline gold are detected in the XRD patterns whatever the gold loading, pointing out the low metal content and/or crystalline domain of the metal particles deposited.

Typical TEM micrographs of the gold catalysts are shown in Fig. 2. In the low loaded solids (Fig. 2b and c), only some few gold particles are visible, with diameters ranging from 5 to 10 nm. Those particles with a very low diameter (typically, below 1 nm) are difficult to be detected due to the low mass and diffraction contrast and must be the majority, in good agreement with the XRD results. The highest loaded catalysts (1.26Au/Ti, Fig. 2a) presents

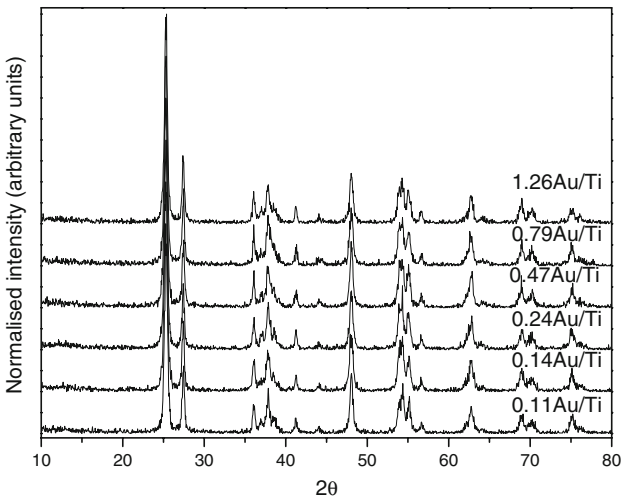

Fig. 1 XRD diagrams of the gold/titania catalysts

a regular distribution of spherical gold particles on the whole support, with diameters ranging from 1.5 to 10 nm. As no diffraction peaks due to polycrystalline gold are observed in its XRD diagram, the existence in this sample of gold particles of lower diameter can be also postulated. In the samples 0.47Au/Ti and 0.79Au/Ti (Fig. 2d), some big particles of about 100 nm are also detected.

Qualitative XPS analyses of the gold samples are similar for all studied solids. Binding energy values found for Au $4f_{7/2}$ and Au $4f_{5/2}$ levels were 83.7 and 87.0 eV, respectively, characteristic of Au^0 species [13, 30]. No oxidised gold species were detected, even in the reacted catalysts, as it can be seen in Fig. 3. This is not surprising provided that the ultrahigh vacuum of the XPS chamber ($<1 \times 10^{-9}$ Torr) is a reducer treatment, which could drive to the reduction of the oxidised gold species. In fact, fresh samples are only dried ones, and the presence of oxidised gold can be postulated since a drying treatment at 100 °C seems to be not enough to reduce all gold. Quantification results evidence the surface enrichment in gold for all samples except for 0.79Au/Ti one, where a higher gold concentration in the bulk is measured (Fig. 4). This agrees with TEM observations of big gold particles on this sample and points out to a low dispersion and high average gold particle size on it. On the other hand,

Table 1 Code, gold content, textural properties of the studied solids

Code	Au content (% w/w)	S_{BET} (m^2 g^{-1})	Pore Volume (cm^3 g^{-1})	Pore diameter (Å)
TiO_2	–	50	0.150	117
0.11Au/Ti	0.11	48	0.223	187
0.14Au/Ti	0.14	49	0.257	208
0.24Au/Ti	0.24	50	0.237	188
0.47Au/Ti	0.47	52	0.251	186
0.79Au/Ti	0.79	50	0.220	177
1.26Au/Ti	1.26	45	0.209	187

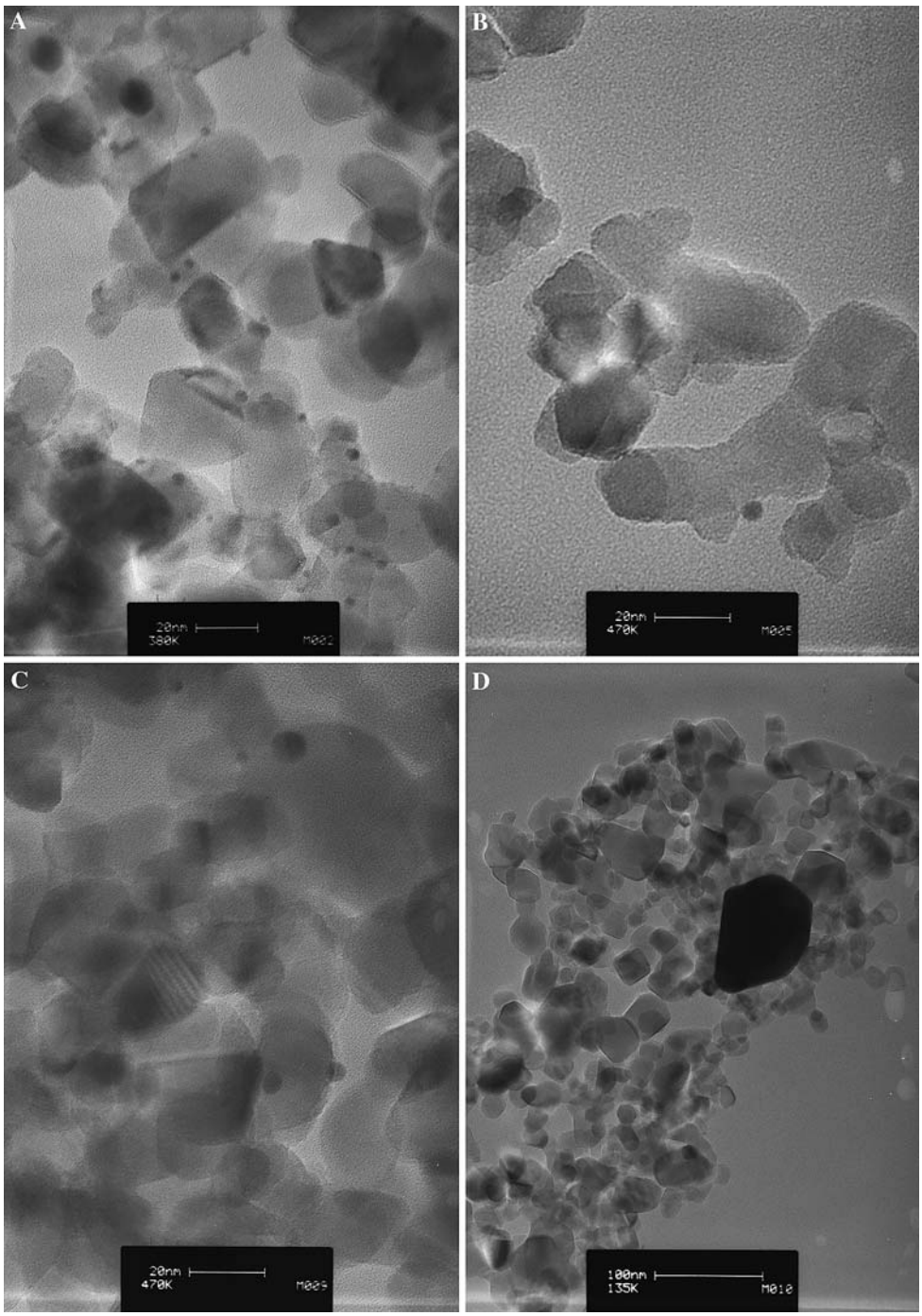

Fig. 2 Typical TEM micrographs of the catalysts studied: (**a**) 1.26Au/Ti; (**b**) 0.14Au/Ti; (**c**) 0.24Au/Ti; (**d**) 0.79Au/Ti

reacted samples have a higher surface gold concentration than fresh ones putting in evidence a surface migration of gold under reaction conditions.

The UV–Vis spectra of the studied solids are shown in Fig. 5. The strong absorption observed at wavelengths lower than 400 nm is assigned to the intrinsic band gap absorption of TiO_2 [14, 31, 32]. The absorption edge shifts toward higher wavelengths for the gold catalysts, pointing out a decrease in the band gap energy of TiO_2 when supporting gold. The most accepted method for determining the band gap energy values of an insulator or semiconductor is by plotting the square root of the Kubelka–Munk function multiplied by the photon energy versus the photon energy and extrapolating the linear part of the rising curve to zero [33−36]. The results are shown in Table 2. The value obtained for the TiO_2 P25 support is 3.0, close to that reported early [32, 36]. Gold catalysts have lower band gap energies, a minimum values being detected for 0.24Au/Ti sample (Fig. 6). The decrease in the band gap energy of a semiconductor oxide when doping with transition metal

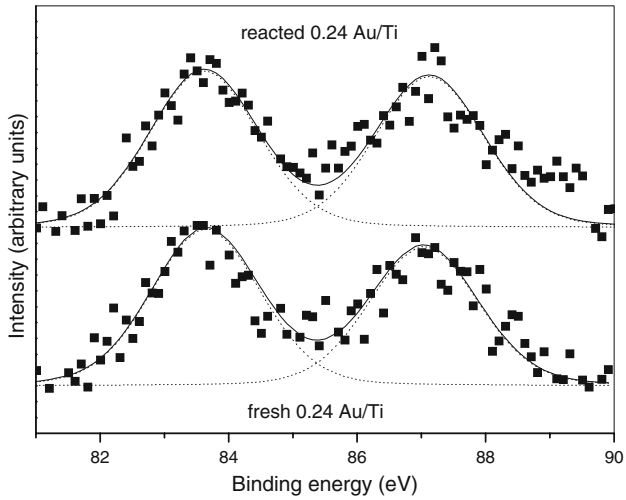

Fig. 3 Typical XPS spectra of the Au4f levels of fresh and reacted in the photocatalytic reaction, 0.24Au/Ti sample

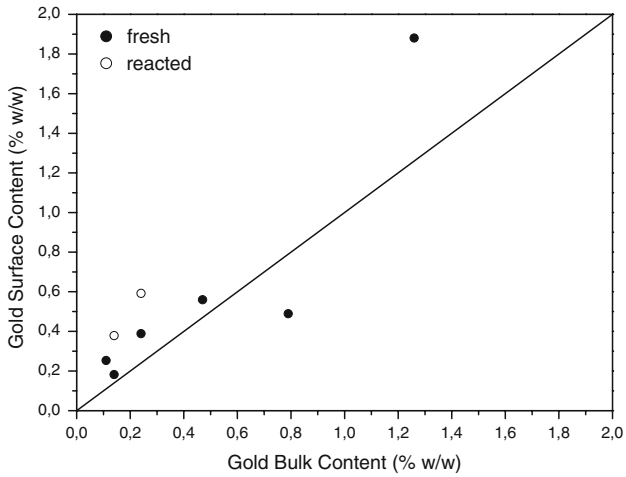

Fig. 4 Relationship between the surface (measured by XPS) and bulk (measured by XRF) gold content on the studied catalysts

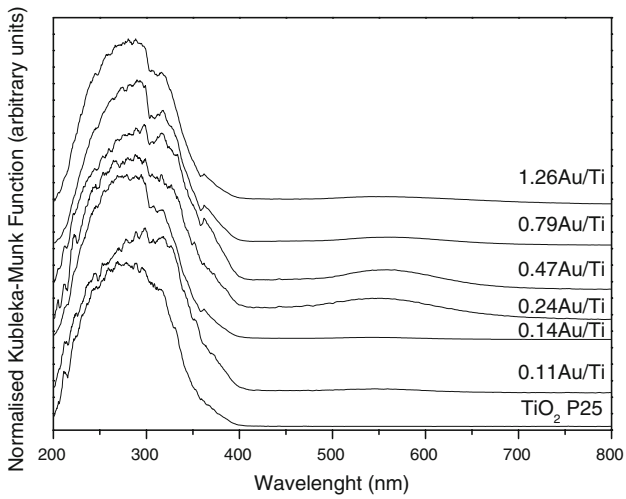

Fig. 5 UV–Vis spectra of the considered solids

Table 2 Band gap energy of the studied solids, calculated from DR UV–Vis measurements

Sample	Band gap (eV)
0	3.0
0.11Au/Ti	2.92
0.14Au/Ti	2.98
0.24Au/Ti	2.80
0.47Au/Ti	2.83
0.79Au/Ti	2.93
1.26Au/Ti	2.98

ions have been reported early in the literature and it is ascribed to the introduction of energy levels in the inter-band gap of the material [37]. This effect has been described early for $Au/CeO_2/Al_2O_3$ [35] and Fe/TiO_2 [31] solids. Besides the band gap absorption of TiO_2, the UV–Vis spectra of the gold samples present a wide band in the 450−700 nm region. This band is due to the surface plasmon resonance of the Au metal particles and it is affected by the gold particle size and shape and the dielectric properties of the surrounding environment [38]. Figure 7 shows the relationship found among the position and area of these bands and the gold content of the solid. As it can be seen, these band features presents a similar behaviour, increasing with the gold loading, and passing through a maximum for gold contents around 0.8%. In fact, if we represent both band characteristics, a linear relation is obtained (Fig. 8). As the dielectric properties of the environment must be considered similar in all solids, these changes must be ascribed mainly to differences in the average gold particle size in the catalysts. If it so, this correlation put in evidence the different gold particle size in the solid, and can be used as indicative of the relative metallic particle size from one sample to another. This is a very important feature, since nor TEM nor XRD have been

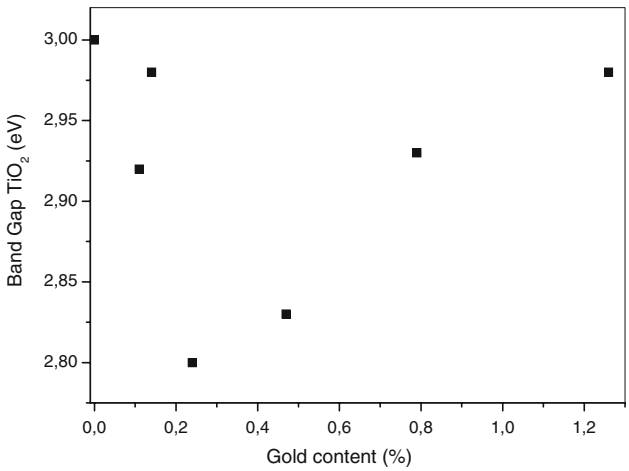

Fig. 6 Relationship between the band gap and the gold content of the studied catalysts

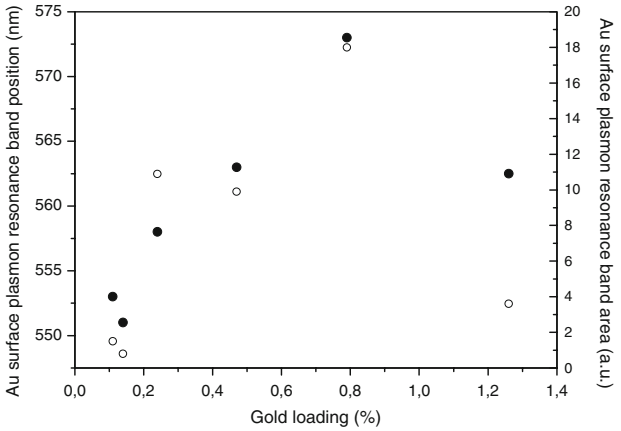

Fig. 7 Relationship between the position (left) and the area (right) of the observed gold surface plasmon resonance UV–Vis band and the gold content on the studied catalysts

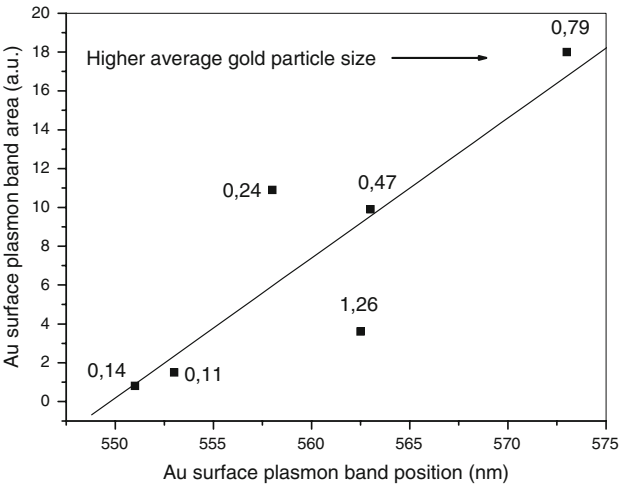

Fig. 8 Relationship between the position and the area of the observed gold surface plasmon resonance UV–Vis band for the studied catalysts

able to give us such clear information. From Fig. 8 it is clear that 0.79Au/Ti and 0.14Au/Ti are those samples with the higher or lower average gold particle sizes, although, from this figure, it is not possible to ascribe them each other. However, we can suspect, that 0.79Au/Ti sample will be the one with the higher average metallic particle size, since we have detected some very big gold particles by TEM micrographs. In the same way, the low gold loading in 0.14Au/Ti sample make easier the obtention of smaller gold particles. It is interesting to note that 1.26Au/Ti sample has a lower gold particle size than that of 0.79Au/Ti and 0.47Au/Ti. This result is not easy to explain. A possible explanation would be the change in the experimental conditions due to the high concentration of the chloroauric acid solution used to prepare the sample. It is well known the strong influence in determining the gold particle size of the control of all the experimental parameters of the deposition–precipitation method. In our case, even having fixed some parameters (pH, temperature, volume of chloroauric solution and time in contact between the support and the gold solution), some others, such as the chloroauric solution concentration, the ratio of its volume and concentration to the mass of support and the volume and time of addition of NaOH to adjust the pH, differs from one preparation to another. Another possibility is that, at so high gold concentration, a change in the equilibrium between the gold adsorbed species and those in solution occurs. If it so, changes in the gold uptake from solution may be observed. Figure 9 shows the differences in gold uptake from solution for the catalysts prepared. From this figure it is clear that 1.26Au/Ti is that with the lowest gold uptake. Moreau et al. [39, 40] have shown that changes in the surface area and crystalline phases of the titania support drives to changes in the gold uptake, which could be related to changes in the number and nature of the sites of gold adsorption. Also, they have evidenced that lower the gold uptake, lower the gold particle size. Our data presented in Figs. 8 and 9 agrees with that conclusion.

3.2 Catalytic Activity

Figure 10 shows the CO conversion as function of temperature of the considered gold catalysts. The highest activity is shown by the solid with the highest gold loading, 1.26Au/Ti, which presents a 100% CO conversion at room temperature. The other gold samples have lower activities, and only 0.79Au/Ti shows some CO conversion (10%) at room temperature. However, there is no a simple and direct relationship between the catalytic activity and the gold content of the sample. For instance, the worst catalytic performances are presented by 0.47Au/Ti sample. In order to compare the activity performances of the catalysts, the

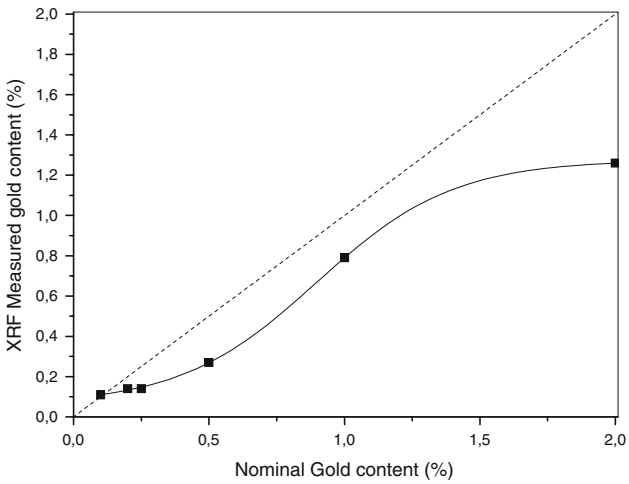

Fig. 9 Relationship between the nominal and real (measured by XRF) gold content on the studied catalysts

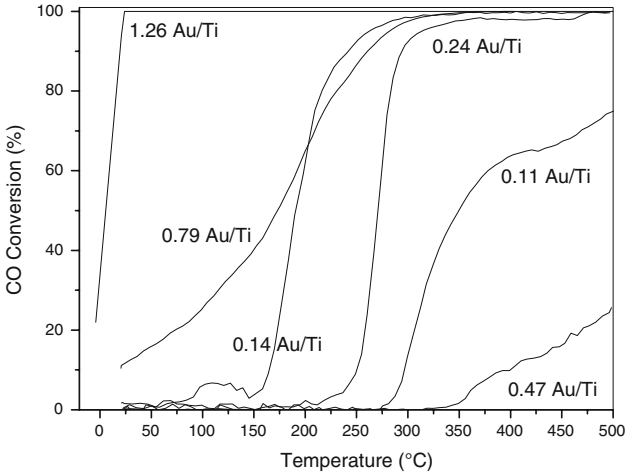

Fig. 10 CO conversion versus temperature for the studied catalysts

temperature at which the 50% of the initial CO is converted into CO_2 (T_{50}) is presented in Fig. 11 as a function of the gold content of the solid. This figure can be explained assuming that the catalytic activity is a function not only of the gold loading, but also of the gold particle size. In fact, gold particle size is considered as the main factor, which determines the activity in gold catalysts [2]. Two different behaviours can be observed. At low gold loadings ($\leq$0.47%), the effect of the gold particle size is more important than the effect of the gold content. In this way, 0.11Au/Ti sample present a T_{50} value of 349°C. The increment in activity observed for 0.14Au/Ti (T_{50} = 192 °C) is due mainly to the decrease in the gold size, since the change in the gold loading is very small. Finally, the activity of the samples 0.24Au/Ti and 0.47Au/Ti (T_{50} = 271 and >500°C, respectively), decreases with the gold loading, being this effect due to the increment in the gold particle size observed in this samples. On the other hand, at gold contents higher than 0.47%, the catalytic activity of the system is controlled by the gold loading, in spite of the particle size of the gold phase.

The results obtained for the photocatalytic activity towards the phenol degradation of the studied catalysts as a function of the gold content are shown in Fig. 12. The activity of the catalysts increases with the gold loading for low metal contents, pass through a maximum for 0.25% Au, and then, decreases linearly at higher gold loadings, being the activity of 1.26Au/Ti sample lower than that of the unmodified TiO_2 P25. Apparently, there is not an influence of the gold particle size in the photocatalytic activity of the samples.

It is well known that noble metal nanoparticles are very effective electron acceptor centres due to the formation of a Schottky junction between the metal and the semiconductor [23, 24]. Acting as sinks for photogenerated electrons, noble metal particles could contribute to the separation of electron–holes pairs reducing the recombination rate and therefore enhancing the photocatalytic efficiency. However, for TiO_2 P25 sample, the junction between its two constituent phases (anatase and rutile) already provides an very good path for electron–hole separation: holes are concentrated in rutile and electrons are left in anatase particles before migration to the particle surface [41–43], thus this mechanism would not have an important contribution to the improvement of activity when specifically P25 is the support for the noble metal, as some works have already pointed out for Pt deposition on titania P25 [41, 43, 44]. On the contrary, Valden et al. have shown that when particles of Au on titania are very small (<3 nm), these behave not longer as metallic but as semiconducting due to a quantum size effect [45]. Then, a mechanism based on semiconductor–semiconductor contact could be proposed in which photogenerated electrons could be injected from

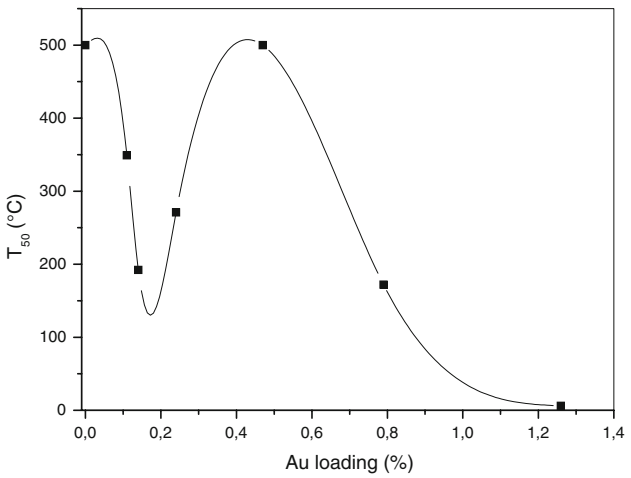

Fig. 11 Temperature at which the 50% CO conversion is obtained, as a function of the gold content of the studied solids

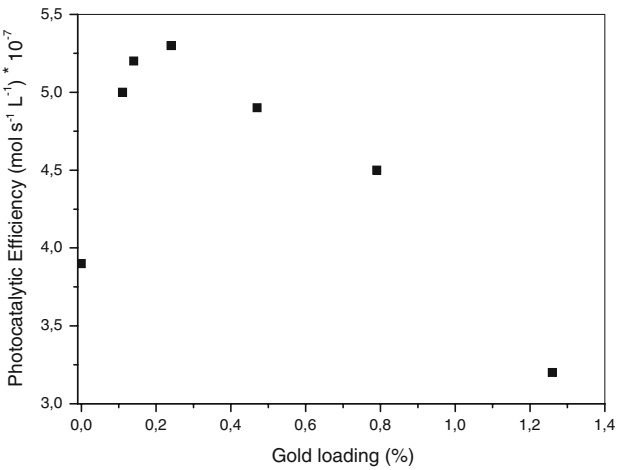

Fig. 12 Phenol photodegradation rate as a function of the gold content of the studied solids

the Au particles into the TiO_2 to contribute in the photocatalytic process, as it has been reported in [15, 46, 47] and very recently in [48]. As TEM and XRD results and Fig. 8 seems to point out, there are very small particle of Au on the different samples, and the improvement on the photoactivity for the samples with Au could be also ascribed to this second mechanism. Thus, the particles with the mean contribution to the enhancement of the activity would be those of small size, having the bigger ones not such an important role on the process and therefore apparently a direct correlation between the activity and the size could not be found, as it has been done in other works [17, 49]. This could be considered as another indirect proof supporting the existence of these very small particles of Au: the only few particles observed by TEM with very large sizes (ca. 100 nm) could scarcely have a positive role in the photocatalytic process.

The increase of activity with the gold content up to a maximum (0.25%) could be due to the increased number of metal nanoparticles, which serves as effective traps and injection centres for electrons. On the other hand, when the concentration of Au particles is high, the active sites of titania could be covered by gold, decreasing the catalytic activity of the system, as observed for high loading of Au particles (Fig. 12). In addition, at high gold contents, Au particles could act as electron–hole recombination centres, decreasing the efficiency of the samples. With respect to the influence of the band gap of the solid in the photocatalytic activity, it is interesting to note that the highest activity is found for the sample with the lower band gap (0.24Au/Ti), as expected (Fig. 13). Therefore, the combination of these effects at high gold contents: blocking titania active sites, electron–hole recombination power of gold metallic centres and the increasing in the band gap energy of the solid, can be claimed as responsible of the maximum in activity detected for a 0.24% gold content. This value is lower than those reported early for Pt, Pd and Au (0.5–1% [23, 43, 50]) or even more [24]. Finally, the effect of others structural parameters, such as S_{BET}, anatase/rutile ratio and TiO_2 average size of the crystalline domains, can be ruled out, since we have shown that they remains practically unaltered.

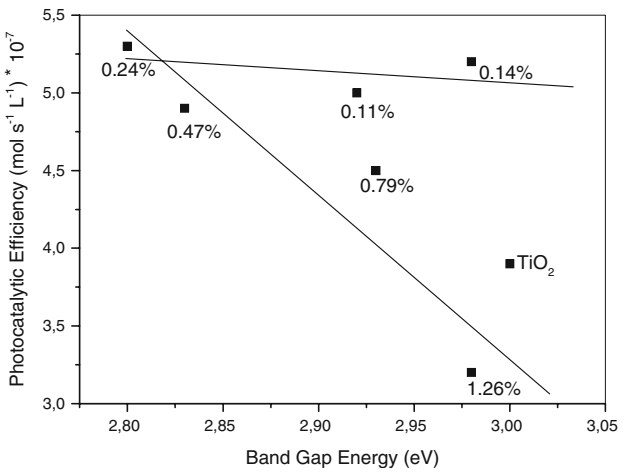

Fig. 13 Phenol photodegradation rate as a function of the band gap of the studied solids

4 Conclusions

In this paper we have studied the catalytic behaviour of a series of Au/TiO_2 samples with gold loadings ranging from 0.11% to 1.26% in the gaseous CO oxidation and photocatalytic degradation of phenol in aqueous media.

For the CO oxidation reaction, the catalysts activity is a function of the gold particle size and gold content, being the effect of the particle size more important at low gold coverage. However, for the photochemical phenol oxidation, the enhancement effect of gold seems to be produced mainly by the small gold particles (<3 nm) deposited on the surface of titania with independence of the size of bigger particles. The photocatalytic activity is then depending on the band gap value of the solid and especially on the gold loading.

Acknowledgments Financial support by Junta de Andalucía (TEP106 and FQM181, PAI) and MCyT (MAT2006-12386-C05-01 and CTQ2004-05734-C02-02) are gratefully acknowledged.

References

1. Bond GC, Thompson DT (1999) Catal Rev-Sci Eng 41:319
2. Haruta M (1997) Catal Today 36:153
3. Gluhoi AC, Lin SD, Nieuwenhuys BE (2004) Catal Today 90:175
4. Zwijnenburg A, Makkee M, Moulijn JA (2004) Appl Catal A 270:49
5. Idakiev V, Tabakova T, Yuan Z-Y, Su B-L (2004) Appl Catal A 270:135
6. Centeno MA, Paulis M, Montes M, Odriozola JA (2002) Appl Catal A 234:65
7. Nijhuis TA, Weckhuysen BM (2006) Catal Today 117:84
8. Valden M, Pak S, Lai X, Goodman DW (1998) Catal Lett 56:7
9. Soares JMC, Morrall P, Crossley A, Harris P, Bowker M (2003) J Catal 219:17
10. Overbury SH, Schwartz V, Mullins DR, Yan W, Dai S (2006) J Catal 241:56
11. Solsona BE, García T, Jones C, Taylor SH, Carley AF, Hutchings GJ (2006) Appl Catal A 312:67
12. Prati L, Rosi M (1998) J Catal 176:552
13. Dimitratos N, Villa A, Bianchi CL, Prati L, Makkee M (2006) Appl Catal A 311:186
14. Sonawane RS, Dongare MK (2006) Mol J Catal A 243:68
15. Orlov A, Jefferson DA, Macleod N, Lambert RM (2004) Catal Lett 92:41
16. Li H, Bian Z, Zhu J, Huo Y, Li H, Lu Y (2007) J Am Chem Soc 129:4538

17. Chan SC, Barteau MA (2005) Langmuir 21:5588
18. Augugliaro V, Litter M, Palmesano L, Soria J (2006) J Photochem Photobiol C 7:127
19. Dillert R, Cassano AE, Goslich R, Bahnemann D (1999) Catal Today 54:267
20. Bahnemann D (2004) Solar Energy 77:445
21. Araña J, Doña-Rodrıguez JM, Garriga i Cabo C, González-Dıaz O, Herrera-Melián JA, Pérez-Peña J (2004) Appl Catal B 53:221
22. Peral J, Domenech X, Ollis DF (1997) J Chem Technol Biotechnol 70:117
23. Sakthivel S, Shankar MV, Palanichamy M, Arabindoo B, Bahnemann D, Murugesan V (2004) Water Res 38:3001
24. Sreethawong T, Yoshikawa S (2005) Catal Commun 6:661
25. Chen X, Mao SS (2007) Chem Rev 107:2891
26. Sakthivel S, Hidalgo MC, Bahnemann DW, Geissen S-U, Murugesan V, Vogelpohl A (2006) Appl Catal B 63:31
27. Heller HG, Langan JR (1981) J Chem Soc, Perkin Trans II 341
28. Kónya Z, Puntes VF, Kiricsi I, Zhu J, Ager JW, Ko MK, Frei H, Alivisatos P, Somorjai GA (2003) Chem Mater 15:1242
29. Domínguez MI, Sánchez M, Centeno MA, Montes M, Odriozola JA (2006) Appl Catal A 302:96
30. Centeno MA, Paulis M, Montes M, Odriozola JA (2005) Appl Catal B 61:177
31. Zhou M, Yu J, Cheng B (2006) J Hazard Mat B 137:1838
32. Gartner M, Dremov V, Muller P, Kisch H (2005) Chem Phys Chem 6:714
33. Tandom SP, Gupta JP (1970) Phys Stat Sol 38:363
34. Weber RS (1995) J Catal 151:470
35. Centeno MA, Portales C, Carrizosa I, Odriozola JA (2005) Catal Lett 102:289
36. Yu J, Zhou M, Cheng B, Zhao X (2006) J Mol Catal A 246:176
37. Navio JA, Hidalgo MC, G. Colón, Botta SG, Litter MI (2001) Langmuir 17:202
38. Mulvaey P (1996) Langmuir 12:788
39. Moreau F, Bond GC, Taylor AO (2005) J Catal 231:1095
40. Moreau F, Bond GC (2006) Appl Catal A 302:110
41. Sun B, Vorontsov AV, Smirniotis PG (2003) Langmuir 19:3151
42. Emilio CA, Litter MI, Kunst M, Bouchard M, Colbeau-Justin C (2006) Langmuir 22:3606
43. Hidalgo MC, Maicu M, Navío JA, Colón G (2007) Catal Today 129:43
44. Lee SK, Mills A (2003) Platinum Metals Rev 47:61
45. Valden M, Lai X, Goodman DW (1998) Science 281:1647
46. Subramanian V, Wolf EE, Kamat PV (2004) J Am Chem Soc 126:4943
47. Tian Y, Tatsuma T (2005) J Am Chem Soc 127:7632
48. Furube A, Du L, Hara K, Katoh R, Tachiya M (2007) J Am Chem Soc 129:14852
49. Iliev V, Tomova D, Bilyarska L, Tyuliev G (2007) J Mol Chem Catal A 263:32
50. Hufschmidt D, Bahnemann D, Testa JJ, Emilio CA, Litter M (2002) J Photochem Photobiol A: Chem 148:223